Current Optics and Photonics
Vol. 4, No. 4, August 2020, pp. 361-367

ISSN: 2508-7266(Print) / ISSN: 2508-7274(Online)
DOI: https://doi.org/10.3807/COPP.2020.4.4.361

Microwave Instantaneous Frequency Measurement (IFM) Approach Based on an Integrated Photonic Ti:$LiNbO_3$ Y Branch

Changsheng Zhang[1,2], Jiahong Zhang[1,2]*, and Zhengang Zhao[1,2]

[1]*Faculty of Information Engineering and Automation, Kunming University of Science and Technology, Kunming 650504, China*
[2]*Yunnan Key Laboratory of Computer Technology Applications, Kunming 650504, China*

(Received February 6, 2020 : revised June 4, 2020 : accepted June 29, 2020)

An approach based on an integrated photonic Ti:$LiNbO_3$ Y branch has been proposed, designed, and analyzed for the microwave instantaneous frequency measurement (IFM). By designing the Y branch with length $L = 6545$ μm and refractive index $N_{TE} - N_{TM} = 0.0764$, a complementary optical filter with free spectral range (FSR) of 600 GHz is constituted, which results in a maximum measureable frequency of 300 GHz being obtained. Theoretical analysis on the temperature stability of the Ti:$LiNbO_3$ Y branch shows that the FSR variation of the complementary filter is 0.3% for the temperature change of 100 K, which indicates that the IFM approach will have a better stability. All these results demonstrate that the proposed IFM approach has potential capability to be used for the increasingly higher microwave IFM with better stability.

Keywords : Microwave photonics, Instantaneous frequency measurement (IFM), Optical waveguide, Optical microwave signal processing
OCIS codes : (120.2440) Filters; (130.0130) Integrated optics; (130.3120) Integrated optics devices; (130.4110) Modulators; (350.4010) Microwaves

I. INTRODUCTION

Microwave (from 300 MHz to 300 GHz) theories and technologies have been extensively researched and widely applied in the civil and defense areas [1]. In electronic warfare, cognitive radio, anti-stealth defense, and electronic intelligence systems, microwave instantaneous frequency measurement (IFM) plays an important role before sending the microwave signals to the specialized receivers for further processing [2]. Compared with the traditional electronics-based methods, the photonics-based IFM approaches have advantages of wider measurement range, faster measurement response, and better immunity to electromagnetic interference (EMI). In the past decade, many kinds of photonics-based IFM approaches have been proposed and extensively researched [3]. Generally, the photonics-based IFM can be implemented by using frequency-to-microwave power mapping [4-6], frequency-to-optical power mapping [7-9], and frequency-to-time mapping [10, 11].

For the approach based on frequency-to-microwave power mapping, two different frequency-dependent microwave power penalty functions are acquired by using the dispersive medium and then the power amplitude comparison function (ACF) is obtained to eliminate the effect of the optical power fluctuation. But, the high speed photo-detector (PD) is required to detect the microwave power [4-6]. For the method based on frequency-to-optical power mapping, only low frequency PD is used to measure the optical power, so the expensive microwave devices are avoided [7-9]. For the technique based on frequency-to-time mapping, the unknown microwave frequency is converted into electrical time delay using a dispersive time delay device [10], or a frequency shifting recirculating delay line (FS-RDL) [11], as a result the technique is capable of measuring the microwave signal with multiple frequencies over a wider

*Corresponding author: zjh_mit@163.com, ORCID 0000-0003-1496-5770
Color versions of one or more of the figures in this paper are available online.

frequency range. But the response time is too long for the instantaneous measurement.

Recently, the integrated photonic assisted IFM methods utilizing the Si_3N_4/SiO_2 optical waveguide add-drop ring resonator [12], optical waveguide micro-ring resonator [13-15], silicon chip [16], silicon photonic integrated Fano resonator [17], and InP integrated ring-assisted Mach-Zehnder interferometer (MZI) [18] are attractive and have been researched intensively, due to the advantages of smaller size, shorter measurement latency, and lower unit cost. However, as the trade-off between the quality factor and the FSR of the ring resonator, the measurement bandwidths of these integrated micro-ring assisted IFM approaches are limited below 40 GHz, which cannot satisfy measurement of the current increasingly higher microwave frequency. Besides, design and fabrication of the integrated photonic ring is somewhat complex and difficult.

In this paper, an IFM approach based on a Ti:$LiNbO_3$ integrated optical waveguide Y branch has been proposed, designed and analyzed. Because the difference of the refractive index between the TE mode and TM mode is very small, the FSR of the proposed complementary optical filter can become larger while the length of the Y branch is only a few millimeters, which can result in measurement range up to hundreds of GHz. In addition, the designing and fabrication of such simple integrated optical waveguide Y branch can be realized relative easily.

II. OPERATION PRINCIPLES

Schematic diagram of the proposed IFM system is shown in Fig. 1. The system consists of a laser diode (LD), a Mach-Zehnder modulator (MZM), a polarization controllable fiber polarizer (Pol), a Ti:$LiNbO_3$ integrated optical waveguide Y branch, two polarization controllable fiber analyzers (Anal), two photo-detectors (PDs), and a microprocessor unit (MPU).

As the Ti:$LiNbO_3$ optical waveguide Y branch is designed and fabricated on the y cut $LiNbO_3$ wafer, both the TE and TM modes are generated, maintained and transmitted in the optical waveguide. The optical phase difference between the two modes is converted to optical intensity at the output of the Anal. By adjusting one of the Anal parallel to the Pol while the other is vertical with the Pol, a complementary optical filter is generated. Two low-frequency PDs are used to convert the two output optical signals to electrical. The voltage ACF can then be obtained by the MPU. Thanks to the complementary transmission responses of the optical filter, a fixed relationship between the microwave frequency and the voltage ACF is established. As a result, the microwave frequency can be identified according to ACF of the output optical power (voltage). The detailed operation principles are as follows:

For the MZM biased at the minimum transmission point, under small signal modulation, the output optical field $E(t)$ can be written as

$$E(t)=\frac{1}{2}\sqrt{P_{in}}J_1(\beta)\left\{e^{j\left[(\omega_c+\omega_m)t+\frac{\pi}{2}\right]}+e^{j\left[(\omega_c-\omega_m)t+\frac{\pi}{2}\right]}\right\}, \quad (1)$$

where P_{in}, ω_c are the power and frequency of the LD output optical signal, $J_n(.)$ denotes the first kind of Bessel function at order of n, $\beta=\pi(V_m/V_\pi)$, V_π are the modulation index and half wave voltage of the MZM, and V_m, ω_m are

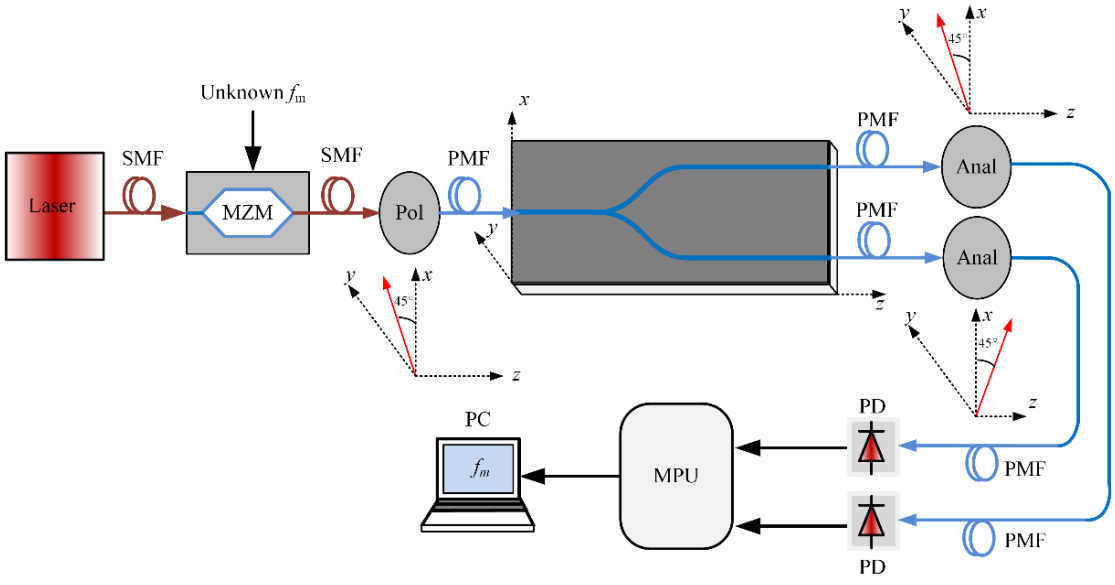

FIG. 1. Schematic diagram of the proposed IFM system: LD, laser diode; f_m, the microwave frequency under measurement; PMF, polarization maintaining fiber; SMF, single mode fiber; MZM, Mach-Zehnder modulator; Pol, polarizer; Anal, analyzer; PD, photo-detector; MPU, microprocessor unit; PC, personal computer.

the amplitude and frequency of the microwave signal to be discriminated.

A linearly polarized light beam is aligned by the polarization controllable optical fiber Pol with an angle of 45° with respect to the x axis of the $LiNbO_3$ crystal, which is projected to the x direction axis (the TE-like mode) and the y axis (TM-like mode) in the Ti:$LiNbO_3$ optical waveguide Y branch. At the output of the Y branch, two polarization controllable fiber analyzers are tuned with angles of 45° (parallel with the Pol) and -45° (vertical with the Pol) with respect to the x axis to convert the optical phase difference into intensity. As a result, a pair of complementary optical filters is established. The transmission response of the complementary optical filter is given by

$$H(\lambda) = 1 \pm \gamma \cos\varphi_0 , \tag{2}$$

where $\gamma = (H_{max} - H_{min}) / (H_{max} + H_{min})$ is the peak-to-valley ratio of the transmission response, H_{max}, H_{min} are the maximum and minimum transmissions, $\varphi_0 = \frac{2\pi}{\lambda}(N_{TE} - N_{TM})L$ is the optical phase difference between the TE and TM mode, λ is wavelength of the LD, L is length of the Y branch, and N_{TE}, N_{TM} are the effective refractive indexes of the TE and TM modes, respectively.

As shown in Fig. 2, consider the optical carrier to be located at ω_c with its offsets $\omega_c - \omega_m$ and $\omega_c + \omega_m$ corresponding to the microwave frequency. The transfer functions given by Eq. (2) can be rewritten as

$$H_P(\omega) = 1 + \gamma \cos(\frac{\omega_m}{F}) , \tag{3a}$$

$$H_V(\omega) = 1 - \gamma \cos(\frac{\omega_m}{F}) , \tag{3b}$$

where $F = \frac{C}{L(N_{TE} - N_{TM})}$ is the free spectral range (FSR) in hertz of the optical filter, and $C = 3 \times 10^8$ m/s is the light speed in the vacuum. By combining Eq. (1) and Eq. (3), the output voltages of the two PDs are given as

$$V_{out1} = P_{in} J_1^2(\beta) \alpha_1 R_1 \left[1 + \gamma \cos(\frac{\omega_m}{F}) \right], \tag{4a}$$

$$V_{out2} = P_{in} J_1^2(\beta) \alpha_2 R_2 \left[1 - \gamma \cos(\frac{\omega_m}{F}) \right], \tag{4b}$$

where α_1, α_2 are the loss coefficients of the two optical paths from the LD to the PDs, R_1, R_2 (unit: V/W) are the voltage conversion coefficients of the two PDs. By adjusting R_1 and R_2 to make it possible that $\alpha_1 R_1 = \alpha_2 R_2$, the voltage ACF can be gotten as

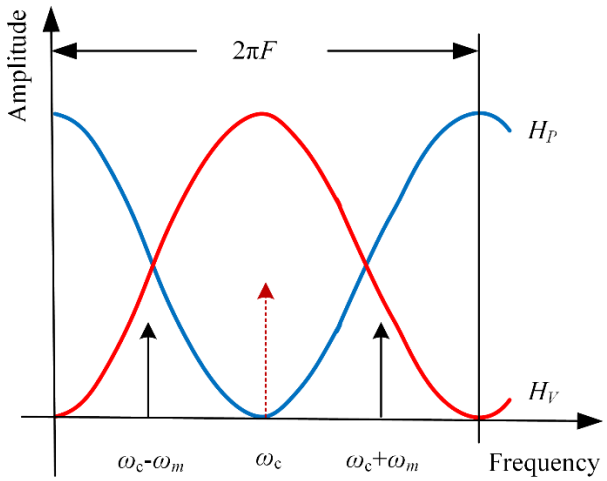

FIG. 2. Transmission responses of the two optical filters.

$$\mathrm{ACF} = \frac{1 - \gamma \cos(\frac{\omega_m}{F})}{1 + \gamma \cos(\frac{\omega_m}{F})} . \tag{5}$$

From Eq. (5), the microwave frequency ω_m and the voltage ACF have a monotonic relationship. As a result, that the microwave frequency can be discriminated by detecting the two output optical powers of the Y branch.

III. CALCULATION RESULTS

3.1. Ti:$LiNbO_3$ Y Branch

As is known, the effective refractive index of the Ti:$LiNbO_3$ optical waveguide is given as [19, 20]

$$N_{TE,TM} = f(\tau, w, t, T) , \tag{6}$$

where τ, w are thickness and width of the pre-Ti strip, and t, T are the diffusion time and temperature. The detailed relationships between N_{TE}, N_{TM} with τ, w, t, and T are given in ref. [19]. Accordingly, by using the pre-Ti strip with different thickness and width, and controlling the diffusion time and temperature, the Ti:$LiNbO_3$ waveguide Y branch with different refractive indices can be fabricated. Consider the maximum detectable microwave frequency $f_{m\max}$ is theoretically equal to $\frac{F}{2}$, the relationship between L, $N_{TE} - N_{TM}$ and $f_{m\max}$ is given by

$$L = \frac{C}{2 f_{m\max}(N_{TE} - N_{TM})} . \tag{7}$$

For $\lambda = 1.53$ μm, to ensure propagation of the fundamental mode, w is designed as 3-7.5 μm, τ is designed as 100 nm, and T, t are controlled at 1050°C and 8.3 h

TABLE 1. Parameters of the designed Ti:$LiNbO_3$ optical waveguide Y branch

w (μm)	τ (nm)	t (h)	T (°C)	λ (μm)	L (μm)	N_{TM} - N_{TE}	F (GHz)	f_{mmax} (GHz)
7	100	8.3	1050	1.53	6545	0.0764	600	300

respectively [20]. Therefore, for N_{TE} - N_{TM} = 0.0764, length of the Ti:$LiNbO_3$ optical waveguide Y branch is designed as 6545 μm to make it possible that the maximum measureable microwave frequency can be up to 300 GHz.

The designed parameters and results are shown in Table 1. In addition, because N_{TE} - N_{TM} is very small, the measurement range of the proposed IFM approach can be up to hundreds of GHz while the length of the Y branch is only a few millimeters.

3.2. Impact of the Relative Peak-to-valley Ratio γ on the IFM Approach

The ACF slopes for different relative peak-to-valley ratios are shown in Fig. 3. As shown in Fig. 3, from DC to 300 GHz, the ACF slopes for γ = 0.6, 0.8 and 1.0 are 12 dB, 19 dB and 105 dB, respectively, which indicates that the measurement resolution for $\gamma \approx 1.0$ is higher than that for γ = 0.6 and 0.8. In contrast, the measurement error is smaller and the measurement range is larger for γ = 0.6 and 0.8 than that for $\gamma \approx 1.0$. This comes from the fact that power of the filtered first sidebands of the microwave signal is larger for γ = 0.6 and 0.8 than that for $\gamma \approx 1.0$, leading to a larger signal-to-noise ratio (SNR) for γ = 0.6 and 0.8. Impact of the peak-to-valley ratio on the filtered first sidebands for $\gamma \approx 1.0$, 0.8 and 0.6 are shown in Fig. 4.

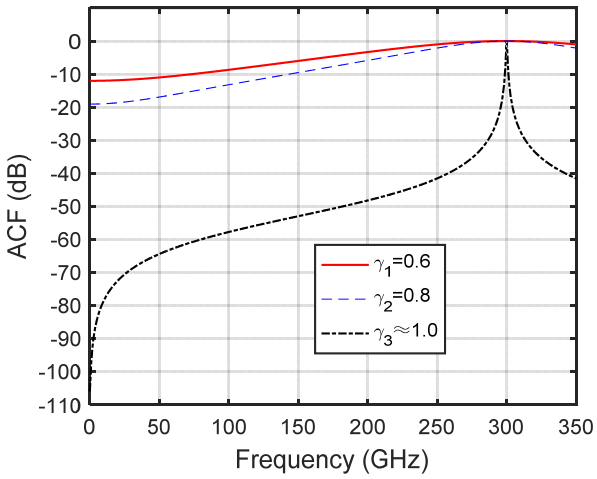

FIG. 3. ACF slopes for different relative peak-to-valley ratios.

Actually, for the proposed IFM approach, the relative peak-to-valley ratio can be given as $\gamma = 2\tan(\theta)/[1 + \tan^2(\theta)]$, which is decided by the polarization angle θ of the input light beam with respect to the y axis. Therefore, the measurement range and resolution can be adjusted by tuning the input polarization angle θ through the polarization controllable fiber Pol.

3.3. Impacts of the Deviation of the Waveguide Refractive Index and Length

In the above analysis, it is assumed that the integrated optical waveguide Y branch works as an ideal complementry optical filter. However, this condition is difficult to implement in a real device since it requires exact Y branch length control for a given TE and TM mode index difference. Moreover, the optical waveguide refractive index difference itself is difficult to control as well. Therefore, impacts of the deviations of the optical waveguide refractive index and length on the ACF have been analyzed. The results are shown in Fig. 5. From Fig. 5(a), when the length deviations change from 50 μm to 300 μm, the maximum measureable frequencies vary from 302.3 GHz to 314.7 GHz, which results in a measurable deviation of 496 MHz/μm. From Fig. 5(b), when the refractive index deviations change from -8×10^{-4} to 8×10^{-4} μm, the maximum measurable frequencies vary from 303.2 GHz to 296.8 GHz, which results a measureable deviation of 337.5 MHz/0.0001. However, in the deviation ranges of both the waveguide refractive index and length, the ACF slope is almost unchanged.

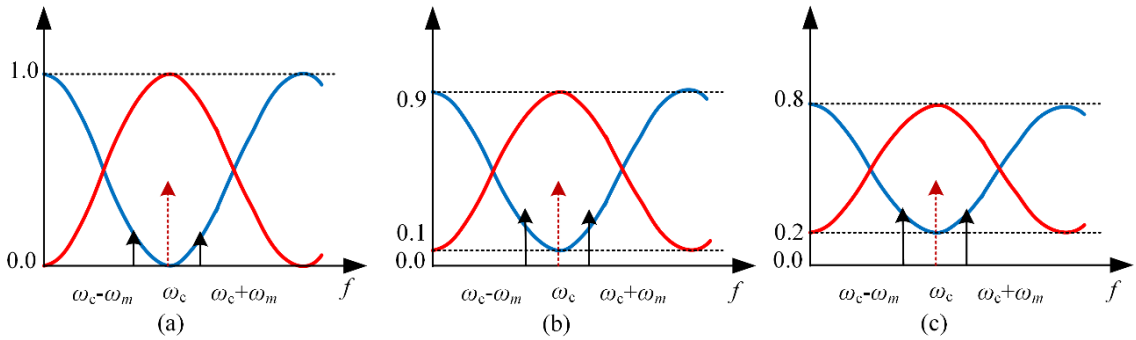

FIG. 4. Impact of the peak to valley ratio γ on the filtered first sidebands: (a) $\gamma \approx 1.0$, (b) γ = 0.8 and (c) γ = 0.6.

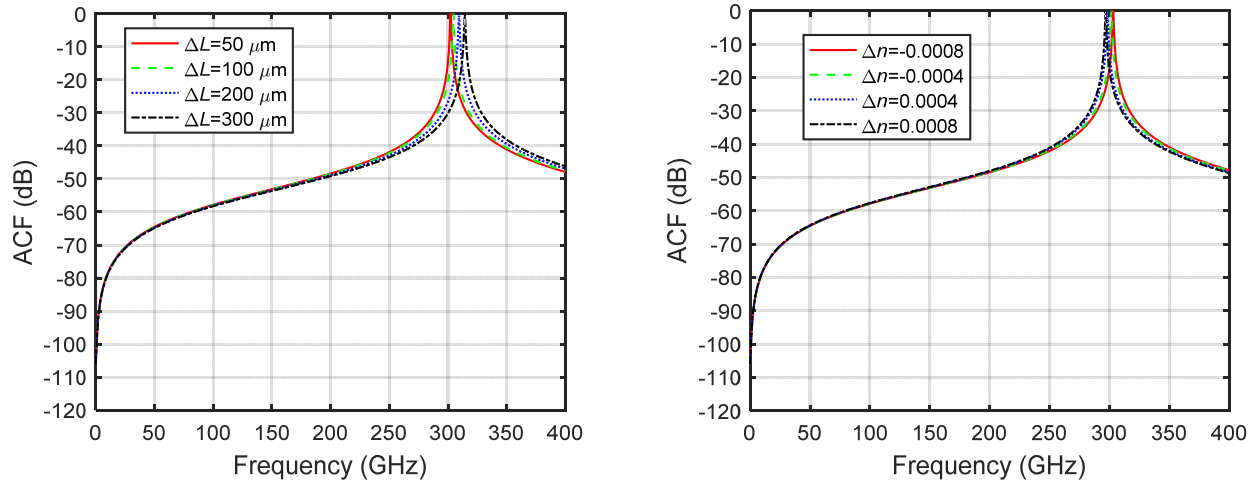

(a) (b)

FIG. 5. Impact of the optical waveguide deviation on the ACF: (a) impact of the waveguide length deviation and (b) impact of the waveguide refractive index deviation.

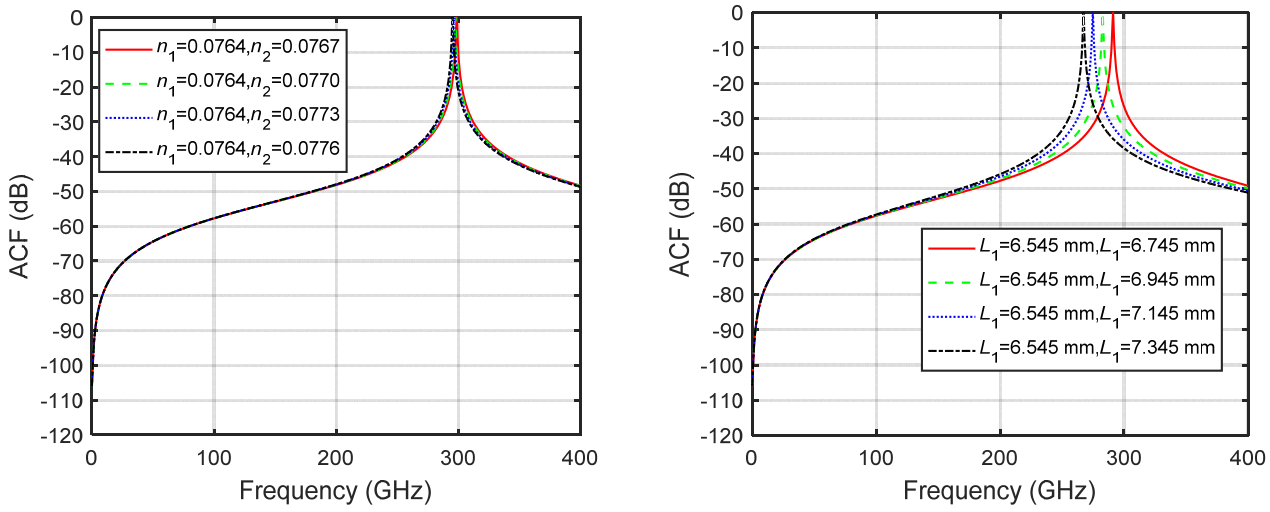

(a) (b)

FIG. 6. Impact of the Y branch asymmetry on the ACF: (a) the refractive index is asymmetric and (b) the length is asymmetric.

3.4. Impacts of the asymmetry of the optical waveguide Y branch

Moreover, for the fabricated $LiNbO_3$ optical waveguides Y branches, it is difficult to ensure properties of the two arms such as the effective refractive index or the waveguide length are symmetric. Therefore, the impacts of the optical waveguide refractive index and length asymmetry on the ACF have been analyzed. The results are shown in Fig. 6. From Fig. 6(a), when the asymmetric refractive indices change from 0.0767 to 0.0776, the maximum measureable frequencies vary from 298.8 GHz to 295.4 GHz. From Fig. 6(b), when the asymmetric waveguide lengths change from 6745 μm to 7345 μm, the maximum measureable frequencies vary from 291.1 GHz to 267.3 GHz. Consequently, the deviation and asymmetry of the optical waveguide Y branch have a strong impct on the IFM range but a little on the ACF slope. However, the best way to investigate these influence factors is to demonstrate the scheme experimentally. But, subject to current experimetal conditions, the integrated optical waveguide Y branch cannot be fabricated for the moment in our laboratory. Therefore, it is necessary to fabricate the optical waveguide Y branch in the near future and to demonstrate the measurement scheme experimentally.

3.5. Stability

As is known, due to the thermo-optic, pyro-electric, photorefractive, and strain-optic effects of $LiNbO_3$ crystal, the stability of $LiNO_3$ integrated optical waveguide devices are affected by the ambient variations, especially by the

ambient temperature [21]. For the proposed IFM approach, as a Ti:$LiNbO_3$ optical waveguide Y branch is designed as a complementary optical filter, the FSR will be affected by the ambient temperature, which in turn affects the frequency measurement performance. Assume $N=(N_{TE}-N_{TM})$, the temperature dependence of F is given as $\frac{\partial F}{\partial T}=-\frac{C}{LN}\left(\frac{1}{L}\frac{\partial L}{\partial T}+\frac{1}{N}\frac{\partial N}{\partial T}\right)$.

For the designed y-cut Ti:$LiNbO_3$ optical waveguide Y branch, $L=6545$ μm, $N=0.0764$, $F=600$ GHz, substituting the thermal expansion coefficient in the z-direction $\frac{1}{L}\frac{\partial L}{\partial T}=7.5\times10^{-6}$ K^{-1}, and the temperature dependence of the birefringence $\frac{1}{N}\frac{\partial N}{\partial T}=2.4\times10^{-5}$ K^{-1} [22] into $-\frac{C}{LN}\left(\frac{1}{L}\frac{\partial L}{\partial T}+\frac{1}{N}\frac{\partial N}{\partial T}\right)$, the temperature dependence of F can be calculated as $\frac{\partial F}{\partial T}=$ -18.9 MHz/K, which results in the change in the FSR error of 0.3% for the temperature change of 100 K. In addition, the pyro-electric effect results in an imbalance of surface charge between the z faces so an electric field $E(T)$ is generated along the optic axis [23]. However, based on the Pockels effect of the $LiNbO_3$ crystal, the refractive index change of the TE and TM mode induced by $E(T)$ is given as $\Delta N_{TE}(E)=\Delta N_{TM(E)}=\frac{1}{2}n_o^3\gamma_{13}E(T)$, accordingly, $\Delta N=\Delta N_{TE}(E)-\Delta N_{TM}(E)=0$, leading no effect on the FSR. Therefore, it can be predicted that the proposed Ti:$LiNbO_3$ optical waveguide Y branch based IFM approach will have better temperature stability.

IV. CONCLUSIONS

An approach based on a Ti:$LiNbO_3$ integrated optical waveguide Y branch has been proposed, designed, simulated and analyzed for the microwave IFM. By designing length of the integrated optical waveguide Y branch is 6.545 mm, the maximum detectable microwave frequency can reach 300 GHz. Impact of the peak-to-valley ratio on the measurement characteristics has been analyzed. The results indicate that the measurement error is smaller and the measurement range is larger for $\gamma=0.6$ and 0.8, while the measurement resolution is higher for $\gamma\approx1.0$. Besides, the measurement range and resolution can be adjusted by tuning the input polarization angle θ through the polarization controllable fiber Pol. In addition, the theoretical analysis on the temperature stability of the Ti:Y branch show that change of the FSR is 0.3% for the temperature change of 100 K. All these results reveal that such an approach has potential capability to be used for the microwave IFM with broad bandwidth, tunable measurement range and better temperature stability.

ACKNOWLEDGMENT

This work was supported by National Natural Science Foundation of China (Grant No. 61765009), the Applied Basic Research Project of Yunnan province (Grant No. 2018FB106), and the Introducing Talent Research Start-up Project of KMUST (Grant No.KKSY201603042).

REFERENCES

1. D. M. Pozar, *Microwave Engineering* (John Wiley & Sons, NJ, USA, 2007).
2. P. W. East, "Fifty years of instantaneous frequency measurement," IET Radar. Sonar Navig. **6**, 112-122 (2012).
3. J. Capmany and D. Novak, "Microwave photonics combines two worlds," Nat. Photon. **1**, 319-330 (2007).
4. L. V. T. Nguyen and D. B. Hunter, "A photonic technique for microwave frequency measurement," IEEE Photon. Technol. Lett. **18**, 1188-1190 (2006).
5. Y. Wang, J. Ni, H. Chi, X. Zhang, S. Zheng, and X. Jin, "Photonic instantaneous microwave frequency measurement based on two different phase modulation to intensity modulation conversions," Opt. Commun. **284**, 3928-3932 (2011).
6. H. Emamiand and M. Ashourian, "Improved dynamic range microwave photonic instantaneous frequency measurement based on four-wave mixing," IEEE Trans. Microw. Theory Tech. **62**, 2462-2470 (2014).
7. H. Chi, X. Zou, and J. Yao, "An approach to the measurement of microwave frequency based on optical power monitoring," IEEE Photon. Technol. Lett. **20**, 1249-1251 (2008).
8. X. Zou, H. Chi, and J. Yao, "Microwave frequency measurement based on optical power monitoring using a complementary optical filter pair," IEEE Trans. Microw. Theory Tech. **57**, 505-511 (2009).
9. J. Zhang, X. Yang, C. Zhu, Z. Zhao, C. Li, and Y. Li, "Instantaneous microwave frequency measurement using an asymmetric integrated optical waveguide Mach-Zenhder interferometer (AMZI)," Optik **169**, 203-207 (2018).
10. T. A. Nguyen, E. H. W. Chan, and R. A. Minasian, "Instantaneous high-resolution multiple-frequency measurement system based on frequency-to-time mapping technique," Opt. Lett. **39**, 2419-2422 (2014).
11. L. V. T. Nguyen, "Microwave photonic technique for frequency measurement of simultaneous signals," IEEE Photon. Technol. Lett. **21**, 642-644 (2009).
12. D. Marpaung, "On-chip photonic-assisted instantaneous microwave frequency measurement system," IEEE Photon. Technol. Lett. **25**, 837-840 (2013).
13. L. Liu, F. Jiang, S. Yan, S. Min, M. He, D. Gao, and J. Dong, "Photonic measurement of microwave frequency using a silicon microdisk resonator," Opt. Commun. **335**, 266-270 (2015).
14. L. Liu, H. Qiu, Z. Chen, and Z. Yu, "Photonic measurement of microwave frequency with low-error based on an optomechanical microring resonator," IEEE Photon. J. **9**, 5503611 (2017).
15. L. Liu, W. Xue, and J. Yue, "Photonic approach for microwave frequency measurement using a silicon microring

resonator," IEEE Photon. Technol. Lett. **31**, 153-156 (2019).
16. M. Pagani, B. Morrison, Y. Zhang, A. Casas-Bedoya, T. Aalto, M. Harjanne, M. Kapulainen, B. J. Eggleton, and D. Marpaung, "Low-error and broadband microwave frequency measurement in a silicon chip," Optica **2**, 751-756 (2015).
17. B. Zhu, W. Zhang, S. Pan, and J. Yao, "High-sensitivity instantaneous microwave frequency measurement based on a silicon photonic integrated fano resonator," J. Lightwave Technol. **37**, 2527-2533 (2019).
18. J. S. Fandiño and P. Muñoz, "Photonics-based microwave frequency measurement using a double-sideband suppressed-carrier modulation and an InP integrated ring-assisted Mach-Zehnder interferometer filter," Opt. Lett. **38**, 4316-4319 (2013).
19. S. Fouchet, A. Carenco, R. Guglielmi, and L. Riviere, "Wavelength dispersion of Ti induced refractive index change in $LiNbO_3$ as a function of diffusion parameters," J. Lightwave Technol. **5**, 700-708 (1987).
20. E. Strake, G. P. Bava, and I. Montrosset, "Guided modes of Ti:$LiNbO_3$ channel waveguides: a novel quasi-analytical technique in comparison with the scalar finite-element method," J. Lightwave Technol. **6**, 1126-1135 (1988).
21. J. P. Salvestrini, L. Guilbert, M. Fontana, M. Abarkan, and S. Gille, "Analysis and control of the DC drift in $LiNbO_3$-based Mach-Zehnder modulators," J. Lightwave Technol. **29**, 1522-1534 (2011).
22. K. H. Hellwege and A. M. Hellwege, "Ferroelectrics and Related Substances: Oxides," in *Numerical Data and Functional Relationships in Science and Technology* (New Series Volume III/16a) Landolt-Bornstein, eds. (Springer-Verlag, NY, USA. 1981).
23. C. H. Bulmer, W. K. Burns, and S. C. Hiser, "Pyroelectric effects in $LiNbO_3$ channel-waveguide devices," Appl. Phys. Lett. **48**, 1036-1038 (1986).